

## New Experimental Limits on Exotic Spin-Spin-Velocity-Dependent Interactions by Using SmCo<sub>5</sub> Spin Sources

Wei Ji,<sup>1</sup> Yao Chen,<sup>2\*</sup> Changbo Fu,<sup>3,†</sup> Ming Ding,<sup>2</sup> Jiancheng Fang,<sup>2</sup> Zhigang Xiao,<sup>1</sup> Kai Wei,<sup>2</sup> and Haiyang Yan<sup>4</sup>

<sup>1</sup>*Department of Physics, Tsinghua University, Beijing, 100084, China*

<sup>2</sup>*School of Instrumentation Science and Opto-electronics Engineering, Beihang University, Beijing, 100191, China*

<sup>3</sup>*INPAC and School of Physics and Astronomy, Shanghai Jiao Tong University, Shanghai Key Laboratory for Particle Physics and Cosmology, Shanghai 200240, China*

<sup>4</sup>*Key Laboratory of Neutron Physics, Institute of Nuclear Physics and Chemistry, CAEP, Mianyang, Sichuan 621900, China*



(Received 11 April 2018; published 28 December 2018)

Despite the great success of the standard model (SM), there still exist mysteries like the nature of dark matter, the strong  $CP$  problems, etc. To solve them, many theories proposed new bosons beyond the SM that can mediate new forces. Here, we report the latest results of searching for possible new long-range spin-spin-velocity-dependent forces (SSVDFs), based on specially designed iron-shielded SmCo<sub>5</sub> spin sources and a spin exchange relaxation free comagnetometer. With help from the similarity analysis method, new constraints on some forms of SSVDFs between electrons have been obtained, which represent up to more than 11 orders of magnitude tighter limits than previous experiments for the force range of 5 cm–1 km.

DOI: [10.1103/PhysRevLett.121.261803](https://doi.org/10.1103/PhysRevLett.121.261803)

*Introduction.*—Many new light bosons, such as axions [1–3], dark photons [4,5], paraphotons [6], familons, majorons [7] and  $Z'$  bosons [8] have been introduced by theories beyond the standard model. If they exist, some of them could be candidates for dark matter [9,10]. Furthermore, the new bosons may mediate new types of long-range fundamental forces, or the so-called fifth forces [8,9]. The possible new forces may break the  $C$ ,  $P$ , or  $T$  (or their combinations) symmetries [3], and they have been suspected to be answers to questions like the strong  $CP$  violation problem [3].

The possibility of the existence of new spin-dependent forces has been extensively investigated experimentally [11,12]. It has been pointed out that any interactions between two fermions, which are mediated by spin zero or spin one bosons, could be classified to 16 terms [8]. Many experimental methods have been used to search for them, including the torsion balance [13–16], the resonance spring [17,18], the spin exchange relaxation free (SERF) comagnetometer [15,19–21], nuclear magnetic resonance based methods [22–24], and other high sensitivity technologies [25–28]. However, the experiments about spin-spin-velocity-dependent forces (SSVDFs) are still rare today [27,29].

Following the notation in Ref. [8,30], the SSVDFs to be studied here are

$$V_{6+7} = \frac{-f_{6+7}\hbar^2}{4\pi m_\mu c} [(\hat{\sigma}_1 \cdot \mathbf{v})(\hat{\sigma}_2 \cdot \hat{\mathbf{r}})] \left( \frac{1}{\lambda r} + \frac{1}{r^2} \right) e^{-r/\lambda}, \quad (1)$$

$$V_8 = \frac{f_8\hbar}{4\pi c} [(\hat{\sigma}_1 \cdot \mathbf{v})(\hat{\sigma}_2 \cdot \mathbf{v})] \frac{e^{-r/\lambda}}{r}, \quad (2)$$

$$V_{15} = -\frac{f_{15}\hbar^3}{8\pi m_1 m_2 c^2} \{(\hat{\sigma}_2 \cdot \hat{\mathbf{r}})[\hat{\sigma}_1 \cdot (\mathbf{v} \times \hat{\mathbf{r}})] + (\hat{\sigma}_1 \cdot \hat{\mathbf{r}})[\hat{\sigma}_2 \cdot (\mathbf{v} \times \hat{\mathbf{r}})]\} \left( \frac{1}{\lambda^2 r} + \frac{3}{\lambda r^2} + \frac{3}{r^3} \right) e^{-r/\lambda}. \quad (3)$$

$$V_{16} = -\frac{f_{16}\hbar^2}{8\pi m_\mu c^2} \{(\hat{\sigma}_2 \cdot \mathbf{v})[\hat{\sigma}_1 \cdot (\mathbf{v} \times \hat{\mathbf{r}})] + (\hat{\sigma}_1 \cdot \mathbf{v})[\hat{\sigma}_2 \cdot (\mathbf{v} \times \hat{\mathbf{r}})]\} \left( \frac{1}{\lambda r} + \frac{1}{r^2} \right) e^{-r/\lambda}, \quad (4)$$

where  $f_n$  is a dimensionless coupling constant,  $\hat{\sigma}_1$ ,  $\hat{\sigma}_2$  are the respective spins of the two particles,  $m_1$ ,  $m_2$  are their respective masses,  $m_\mu$  is their reduced mass, and  $\mathbf{v}$  is the relative velocity between the two interacting fermions. It could be found that  $V_{6+7}$  violates time-reversal symmetry ( $T$ ),  $V_{15}$  violates both parity ( $P$ ) and  $T$  symmetries, and  $V_{16}$  violates  $P$  symmetry. Careful studies on those potentials may give clues for fundamental physical questions like the strong  $CP$  violation problem, the arrow of time, etc.

*Published by the American Physical Society under the terms of the Creative Commons Attribution 4.0 International license. Further distribution of this work must maintain attribution to the author(s) and the published article's title, journal citation, and DOI. Funded by SCOAP<sup>3</sup>.*

In Ref. [31], an experimental scheme with high electron spin-density sources, iron-shielded SmCo<sub>5</sub> (ISSCs), was proposed to detect the SSVDFs. By taking advantage of the high electron spin density of ISSC and the high sensitivity of the SERF comagnetometer [32–36], the proposed system had a potential to detect the SSVDFs with record sensitivities. In this Letter, we report new experimental studies on the SSVDFs by using ISSCs and a SERF comagnetometer.

*The SERF's response to the SSVDFs.*—Here, we take  $V_{16}$  as an example. For this new interaction, the corresponding effective magnetic field  $\mathbf{B}_{\text{eff}}$  experienced by the polarized spin due to the spin source can be deduced from  $V_{16} = -\boldsymbol{\mu} \cdot \mathbf{B}_{\text{eff}}$ , where  $\boldsymbol{\mu}$  is the magnetic moment of the probing particle. In a typical polarized noble gas experiment, the probe particles could be nuclei, e.g.,  $^{21}\text{Ne}$ , or valence electrons of alkali.

If this  $\mathbf{B}_{\text{eff}}$  exists, the SERF's response can be estimated by the Bloch equations [32]

$$\frac{\partial \mathbf{P}^e}{\partial t} = \frac{\gamma_e}{Q(P^e)} [\mathbf{B}_{\text{eff}}^e + \mathbf{B} + \beta M^n \mathbf{P}^n + \mathbf{L}] \times \mathbf{P}^e + \frac{P_0^e \hat{\mathbf{z}} - \mathbf{P}^e}{T_e Q(P^e)}, \quad (5)$$

$$\frac{\partial \mathbf{P}^n}{\partial t} = \gamma_n [\mathbf{B}_{\text{eff}}^n + \mathbf{B} + \beta M^e \mathbf{P}^e] \times \mathbf{P}^n + \frac{P_0^n \hat{\mathbf{z}} - \mathbf{P}^n}{\{T_{2n}, T_{2n}, T_{1n}\}}, \quad (6)$$

where  $\mathbf{B}_{\text{eff}}^{e,n}$  are the effective magnetic fields due to the possible new SSVDFs coupling to the electron (or nucleon) spin;  $\mathbf{P}^{e,n}$  are the polarization of electron or nucleon, respectively;  $\mathbf{B}$  is the external magnetic field;  $T_e$ ,  $T_{1n}$ , and  $T_{2n}$  are the electron spin's relaxation time and the nucleon spin's longitudinal and transverse relaxation times, respectively;  $M^{e,n}$  are the magnetization associated with the electron or the nucleon spin;  $P_0^e$  ( $P_0^n$ ) is the equilibrium polarization of the electron (nucleon);  $\beta = 8\pi\kappa/3$ , and  $\kappa$  is approximately equal to 36 for Rb and  $^{21}\text{Ne}$  pair, which are utilized in this experiment [33];  $\mathbf{L}$  is the pumping light induced effective magnetic field experienced by the electron spin;  $Q(P^e)$  is the electron slow-down factor associated with the hyperfine interaction and spin-exchange collisions [32]; and  $\gamma_e$  ( $\gamma_n$ ) is the gyromagnetic ratio of the electron (nucleon). It is worth noticing that Eqs. (5) and (6) are coupled together. For example, if  $B_{\text{eff}}^n = 0$ , but  $B_{\text{eff}}^e \neq 0$ , the SERF still has nonzero output  $S^{\text{sim}}(t)$ .

By solving the equation set (5) and (6) numerically, one can convert the variable  $\mathbf{B}_{\text{eff}}^{e,n}$  or  $\mathbf{B}$  to the SERF's response  $\mathbf{P}^e(t)$ . The numerical results, together with the experimental measurements, are shown in Fig. 1. Here, the applied magnetic fields  $\mathbf{B}_x$  and  $\mathbf{B}_y$  were sinusoidal, and generated by coils located in the SERF's  $\mu$ -metal shielding. Detailed descriptions can be found in Ref. [37]. One can find, in Fig. 1, that the comagnetometer's sensitivity was frequency dependent.

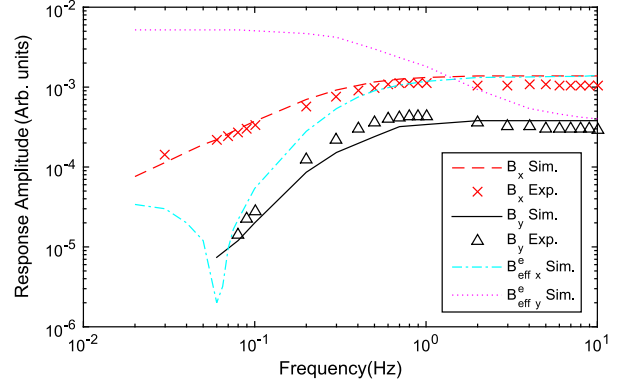


FIG. 1. SERF's response to magnetic fields. The red crosses and red dashed line are experimental and simulation results for  $B_x$ , respectively, while the black triangles and black solid line are for  $B_y$ . The simulation results were obtained by solving Eqs. (5) and (6) numerically. The pink dotted line and blue dashed-dotted line are simulations with assumptions that the exotic force only affected electrons.

*Experimental Setup.*—The experiment was carried out at Beihang University, Beijing, China. The setup is shown in Fig. 2, schematically. The left side is a SERF comagnetometer. A detailed description of the device can be found in Ref. [33]. A spherical aluminosilicate glass vapor cell with a diameter of 14 mm was located at the center of the SERF. It was filled with 3 bar of  $^{21}\text{Ne}$  gas (isotope enriched to 70%), 53 mbar of  $\text{N}_2$  gas, and a small amount of K-Rb mixture. The mixture mole ratio was about 0.05 for the hybrid pumping purpose [36]. The cell was shielded by four layers of  $\mu$  metal and a layer of 10-mm-thick ferrite [38] magnetic field shielding to reduce the ambient magnetic field.

As shown in Fig. 2, a linearly polarized probe laser beam, which was modulated by a 50 kHz signal, passed

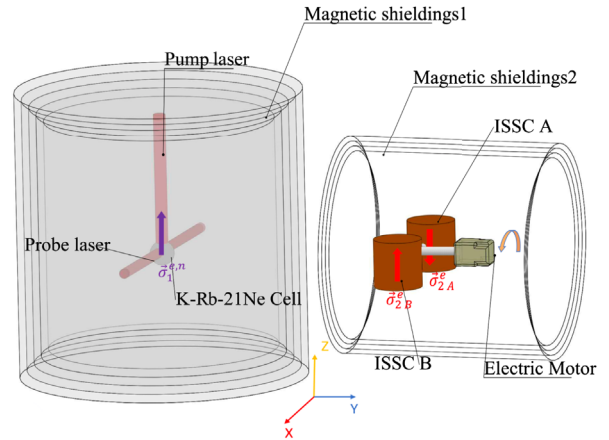


FIG. 2. The experimental setup. The left side was the SERF comagnetometer. The two ISSC spin sources noted as 2A and 2B were driven by a servo motor, and they could rotate clockwise and counterclockwise along the  $y$  axis with a given frequency.

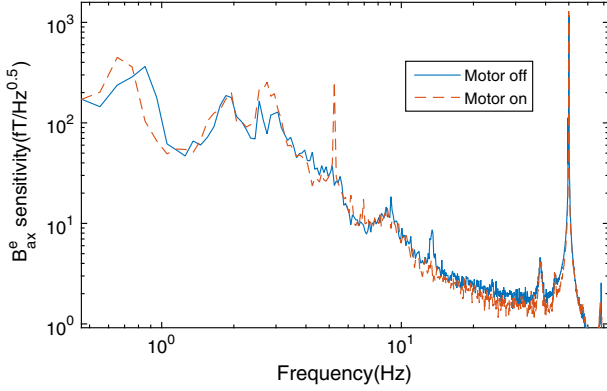


FIG. 3. Typical power spectra measured in the experiment when the driving motor was on (red dashed line) or off (blue solid line). The ISSCs rotated in the frequency of 5.25 Hz, and the motor power system may cause the peak at 5.25 Hz in the spectrum. The 50 Hz peak in the spectrum came from the power supply of the equipment, which was 50 Hz, 220 V. The peak at 13.5 Hz showing up sporadically might be due to an electrical device nearby. The whole SERF system is mounted on a vibration isolation table.

through the cell, and its Faraday rotation angle was then measured using photoelastic modulation. The signals from photodiodes were amplified by a lock-in amplifier, which had a reference frequency of 50 kHz, the same as the probe's modulation. The lock-in output was then recorded by a data-acquisition system.

As shown at the right side in Fig. 2, there were two ISSCs, the electron spin sources. They were identical iron-shielded SmCo<sub>5</sub> magnets [31]. Each ISSC had a cylindrical SmCo<sub>5</sub> magnet inside, which was covered by three layers of pure iron. The magnets were cylindrical with a diameter of 40.00 mm and a height of 40.00 mm. Thicknesses of the iron shielding layers were 15.00, 5.00, and 5.00 mm, respectively. The internal magnetic field of the SmCo<sub>5</sub> magnet was about 1 T.

Driven by a servo motor, the ISSCs rotated clockwise or counterclockwise with a frequency of  $f_0 = 5.25$  Hz. Because the two ISSCs were mounted centrosymmetrically, the dominated frequency of the possible SSVDF signals detected by the SERF was doubled, i.e., 10.5 Hz. This frequency was chosen due to the fact that the SERF comagnetometer had relatively large responses to both  $B_{\text{eff},x}^e$  and  $B_{\text{eff},y}^e$  (Fig. 1), as well as relatively low noise level here (Fig. 3). When rotating to a given angle, the ISSCs could trigger an optoelectronic pulse, and this signal was recorded by the data-acquisition system. This signal was used as the starting point of a new cycle for data analysis. Similar to the SERF, the ISSCs as well as the servo motor were both shielded by four layers of  $\mu$  metal to further reduce possible magnetic field leakage from the ISSCs and servo motor. The signals were recorded continuously for 30 minutes, and then saved as one data set. Between two data sets, the rotation direction or other parameters may be changed if needed.

*Data analysis.*—The experimental data were recorded as  $\mathbf{S}_{i,\text{raw}}^{\text{exp}}(t_j)$ , where  $i$  and  $j$  mean the  $j$ th point in the  $i$ th cycle,  $t_j = j * \Delta t$ , and  $\Delta t = 1$  ms is the data sampling period. Then,  $\mathbf{S}_{i,\text{raw}}^{\text{exp}}(t_j)$  was first transformed to a frequency domain by using fast Fourier transformations (FFTs). A typical SERF power spectrum is shown in Fig. 3. Then, Gaussian filters were applied to remove the peaks corresponding to 5.25 and 50 Hz. After that, the signals were transformed back to the time domain with inverse FFT. Then, dc components in  $\mathbf{S}_{i,\text{raw}}^{\text{exp}}(t_j)$  were also removed. After the steps above, the raw signals  $\mathbf{S}_{i,\text{raw}}^{\text{exp}}(t_j)$  were transferred to  $\mathbf{S}_i^{\text{exp}}(t_j)$  for further analysis.

Expected signals  $S^{\text{sim}}(t)$  sensed by the SERF could be simulated by solving the equation sets (5) and (6) with the experimental parameters and a tentative coupling constant  $f_{16}^{\text{sim}}$  in  $V_{16}$  as inputs. Here, the input  $B_{\text{eff}}$  in Eqs. (5) and (6) was obtained by integrating over the volumes of the ISSCs

$$\mathbf{B}_{\text{eff}} = \frac{f_{16} \hbar^2}{8\mu\pi m_\mu c^2} \iiint \rho(\mathbf{r}) \{ (\hat{\boldsymbol{\sigma}}_2 \cdot \mathbf{v})(\mathbf{v} \times \hat{\mathbf{r}}) + \mathbf{v} [\hat{\boldsymbol{\sigma}}_2 \cdot (\mathbf{v} \times \hat{\mathbf{r}})] \} \times \frac{(r + \lambda) e^{-r/\lambda}}{\lambda r^2} \mathbf{dr}, \quad (7)$$

where  $\mathbf{v}(\mathbf{r}) = \boldsymbol{\omega} \times \mathbf{r}$ ,  $\rho(\mathbf{r})$  is the ISSCs' spin density at location  $\mathbf{r}$ ,  $\boldsymbol{\omega}$  is the angular velocity of the ISSCs. In the parameter space that we were interested in, i.e.,  $B_{\text{eff}} < 1$  nT,  $P_x^e(t)$  approximately linearly depended on  $B_{\text{eff}}$  and, thereafter, the coupling constant  $f_{16}$ . The  $S^{\text{sim}}(t)$  then linearly depended on  $B_{\text{eff}}$ , i.e.,  $S^{\text{sim}}(t) \simeq \eta f_{16}^{\text{sim}} B_{\text{eff}}$ , where  $\eta$  is the calibration constant, which was measured to be  $110 \pm 5$  V/nT. The input  $B_{\text{eff}}$  for solving Eqs. (5) and (6) were simulated by the finite element analysis method [31]. Two examples of simulated signals for  $V_{16}$ , the  $\mathbf{S}_{16}^{\text{sim}}$ , with motor rotating clockwise and counterclockwise are shown in Fig. 4(a).

The experimental signals  $\mathbf{S}_i^{\text{exp}}(t_j)$  were then compared with the simulated ones  $S^{\text{sim}}(t)$ . A cosine similarity score  $k_i$  was used to weigh the similarity between  $\mathbf{S}_i^{\text{exp}}$  and a given reference signal  $\mathbf{S}^{\text{sim}}(t)$ , which can be written as [39]

$$k_i \equiv \frac{\sum_j \mathbf{S}_i^{\text{sim}}(t_j) \cdot \mathbf{S}_i^{\text{exp}}(t_j)}{\sqrt{\sum_j [\mathbf{S}_i^{\text{sim}}(t_j)]^2} \sqrt{\sum_j [\mathbf{S}_i^{\text{exp}}(t_j)]^2}}. \quad (8)$$

The coupling constant in  $V_{16}$  measured experimentally in  $i$ th cycle,  $f_{i,16}^{\text{exp}}$ , can be written as

$$f_{i,16}^{\text{exp}} = k_i f_{16}^{\text{sim}} \sqrt{\frac{\sum_j [\mathbf{S}_i^{\text{exp}}(t_j)]^2}{\sum_j [\mathbf{S}_i^{\text{sim}}(t_j)]^2}}. \quad (9)$$

Distributions of  $f_{i,16}^{\text{exp}}$  are shown in Fig. 4(b). They agree with Gaussian shapes well.

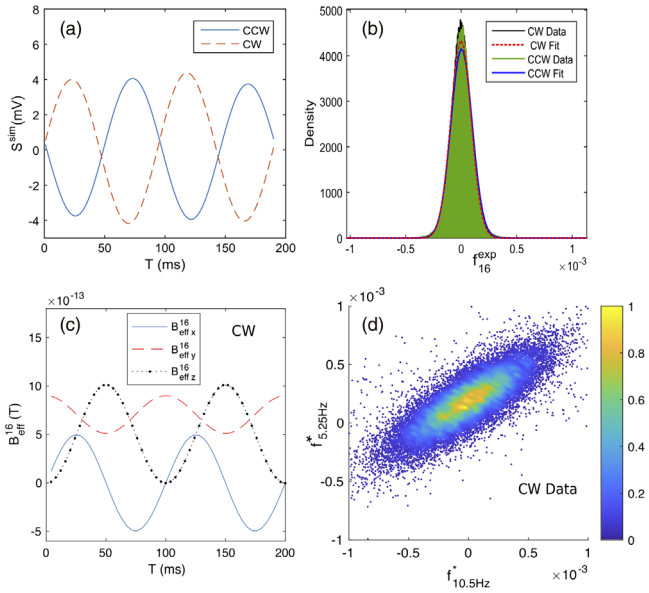


FIG. 4. (a) The simulated  $S_{16}^{\text{sim}}$  signals when motor rotates clockwise (CW) (blue solid line) and counterclockwise (CCW) (red dashed line). (b) The distribution of the  $f_{i,16}^{\text{exp}}$  for  $V_{16}$ . The black area represents the ISSCs rotating clockwise, and green area counterclockwise. The red dashed line and blue solid line are their Gaussian fit, respectively. (c) The  $x$  (blue solid line),  $y$  (red dashed line), and  $z$  components (black dashed-dotted line) of the simulated  $B_{\text{eff}}^{16}$  when the motor rotates clockwise. In subfigures (a), (b), and (c), the following parameters are taken:  $f_{16}^{\text{sim}} = 1 \times 10^{-4}$  and  $\lambda = 1000$  m. (d) The correlation between  $f_{5.25 \text{ Hz}}$  and  $f_{10.5 \text{ Hz}}$ , where take  $S_A^{\text{sim}} = \sin[5.25 \text{ Hz } t]$  or  $S_B^{\text{sim}} = \sin[10.5 \text{ Hz } t]$ , respectively, in Eq. (9).

The final experimentally measured coupling constant  $f_{16}^{\text{exp}}$  was obtained by averaging all rotating cycles including clockwise and counterclockwise, i.e.,

$$f_{16}^{\text{exp}} = \frac{\langle f_{i,16}^{\text{exp}} \rangle_+ + \langle f_{i,16}^{\text{exp}} \rangle_-}{2}, \quad (10)$$

where  $\langle f_{i,16}^{\text{exp}} \rangle_+ = (1/n) \sum_{i=1}^n f_{i,16}^{\text{exp}}$  is the average over the clockwise cycles, and  $\langle f_{i,16}^{\text{exp}} \rangle_-$ , the counterclockwise cycles.

**Results and discussion.**—The other terms of SSVDFs were analyzed by the same method. The parameters of the setup and their errors are shown in Table I. Considering these errors, together with the statistical error, the constraints on the SSVDFs between two electrons could be set. The results are shown in Fig. 5. The gray areas are excluded with 97.7% confidence level. For  $V_{6+7}$ ,  $V_8$ ,  $V_{15}$ , and  $V_{16}$ , our experiment can set new record limits at the range of 5 cm–1 km. Especially for  $V_{15}$ , our result is over 3 orders of magnitude better than [29] in this force range. And for  $V_8$ , our result is more than 11 orders of magnitude better than [27] in the force range of longer than 1 m.

The error budget for  $f_{i,16}^{\text{exp}}$  at  $\lambda = 1.1$  m is shown in Table I. The major systematic error came from the cross talking between the servo motor power system and the

TABLE I. The experimental parameters and their error budgets. The origin of coordinates was at the center of the pumping cell.

Parameter	Value	$\Delta f_{16}^{\text{exp}} (\times 10^{-8})^a$
ISSC net spin ( $\times 10^{24}$ )	$1.75 \pm 0.21$	$-0.32$ $+0.34$
Misalignment (deg)	$< 2$	$< 0.004$
Position of ISSCs $y$ (m)	$-0.624 \pm 0.005$	$+0.13$ $-0.12$
Position of ISSCs $z$ (m)	$0.278 \pm 0.005$	$\pm 0.04$
D between 2 ISSCs(m)	$0.251 \pm 0.001$	$\pm 0.03$
Rotating frequency(Hz)	$5.250 \pm 0.001$	$< 0.001$
Calib. const. $\kappa$ (V/ nT)	$330 \pm 20$	$\pm 0.23$
Phase uncertainty (deg)	$\pm 5$	$\pm 0.27$
Final $f_{16}^{\text{exp}} (\times 10^{-8})$	4.0	$\pm 1.9$ (statistic)
( $\lambda = 1.1$ m)		$\pm 0.5^b$

<sup>a</sup>The contribution to the error budget of  $V_{16}$  at  $\lambda = 1.1$  m

<sup>b</sup>Error contribution from the uncertainties of the parameters listed above.

SERF system. The 5.25 Hz peak shown in Fig. 3 might come from cross-talking effect. However, the major frequency considered here was 10.5 Hz, whose amplitude was about 40 times smaller than 5.25 Hz. The secondary harmonics of 5.25 Hz could also contribute to systematic error. In fact, the correlation between 5.25 and 10.5 Hz could be calculated by applying  $S_A^{\text{sim}}(t_j) = \sin[5.25t_j]$  or  $S_B^{\text{sim}}(t_j) = \sin[10.5t_j]$  to Eq. (9), respectively. As is shown in Fig. 4(d), a correlation between 5.25 and 10.5 Hz was, indeed, found this way, which confirmed the cross-talking effect. The cross talking was the dominant effect in our experiment.

Another major consideration was the magnetic leakage from the ISSCs. With the iron shielding, at a distance of 20 cm away from the ISSC's mass center, its residual magnetic field was measured to be  $< 10$  mG. The magnetic shielding factors for the  $\mu$  metals outside the ISSCs were measured to be  $> 10^6$ , and shielding for the SERF magnetometer,  $> 2 \times 10^6$ . Considering all factors together, we conservatively expect the magnetic leakage from the ISSCs to the SERF's center to be smaller than  $10^{-2}$  aT, which was insignificant in regards to the error budget.

It is worth pointing out that only the errors of the parameters when doing the calculation of  $f^{\text{sim}}$ , as well as the statistical uncertainty, could affect the limit curves drawn in Fig. 5. The magnetic field leakage and cross talking were not subtracted directly. However, their signals might have different waveforms from the expected exotic SSVDF signals, which resulted in relatively smaller cosine similarity scores shown in Eq. (8). By this way, these backgrounds could be partially removed.

**Summary.**—In summary, by using specially designed iron-shielded  $\text{SmCo}_5$  permanent magnets, a high electron spin density source of about  $1.7 \times 10^{21} \text{ cm}^{-3}$  has been achieved, while still keeping its magnetic leakage down to about mG level. The similarity analysis has been proved to

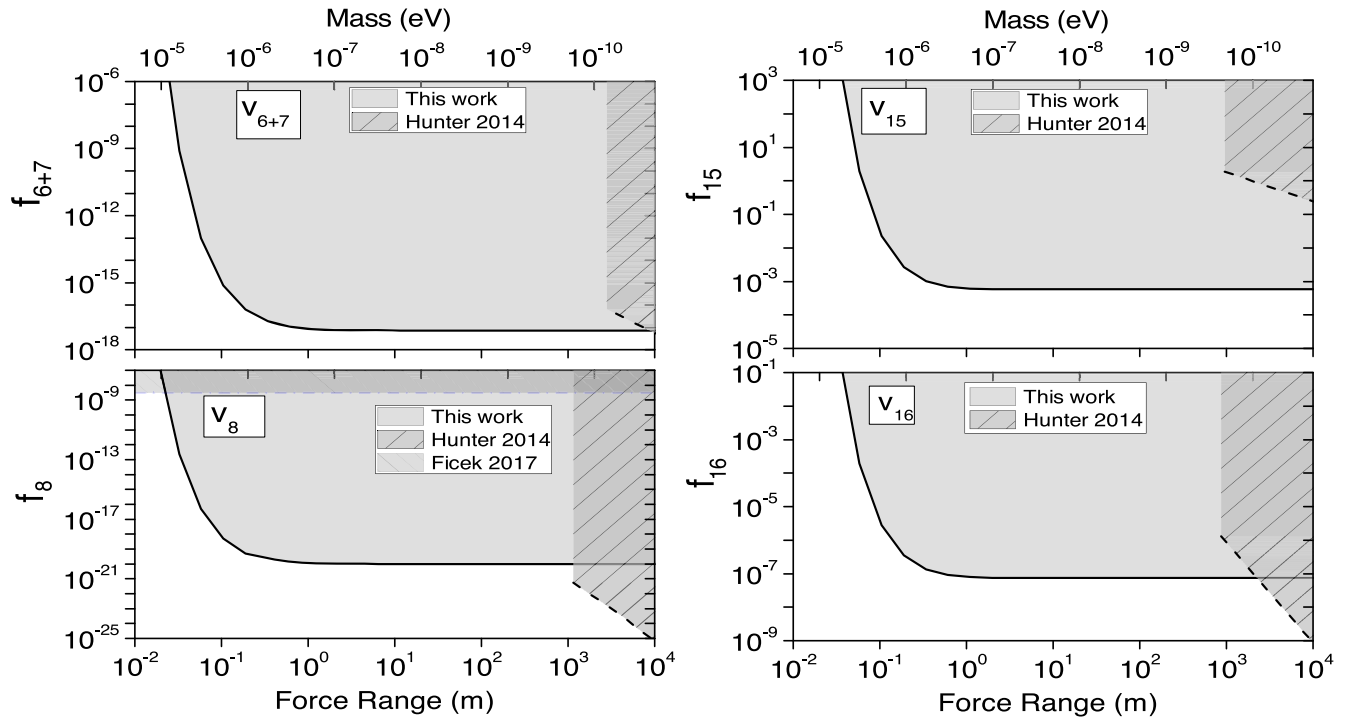


FIG. 5. Limits on the SSVDFs' coupling constants between two electrons measured in this work, which are compared with those in literature. The “Hunter2014” comes from Ref. [29], in which polarized geoelectrons were used. The “Ficek 2017” in the  $V_8$  plot is from [27].

be successful, which gives a significant boost to the detecting sensitivities. With help from the high spin density, the high sensitivity SERF comagnetometer, and the similarity analysis, new constraints on possible new exotic potentials of  $V_{6+7}$ ,  $V_8$ ,  $V_{15}$ , and  $V_{16}$  were derived for the force range of 5 cm–1 km. Especially for  $V_8$ , our result is more than 11 orders of magnitude tighter than previous results in Ref. [27]. By dedication to improving the SERF sensitivities and reducing the crossing-talking effect, a higher sensitivity by a factor of over 1000 is expected in future studies with a similar experimental setup.

This work is supported by the Tsinghua University Initiative Scientific Research Program, the Science Challenge Project (Grant No. TZ2018005), and the National Natural Science Foundation of China (NSFC) under Grants No. 11875191, No. 91636103, and No. 11675152. This work is also supported by the Key Programs of the NSFC under Grant No. 61227902.

\*Corresponding author.  
yao.chen@buaa.edu.cn

†Corresponding author.  
cbfu@sjtu.edu.cn

[1] F. Wilczek, *Phys. Rev. Lett.* **40**, 279 (1978).

[2] S. Weinberg, *Phys. Rev. Lett.* **40**, 223 (1978).

[3] R. D. Peccei and H. R. Quinn, *Phys. Rev. Lett.* **38**, 1440 (1977).

[4] J. Jaeckel and A. Ringwald, *Annu. Rev. Nucl. Part. Sci.* **60**, 405 (2010).

[5] H. An, M. Pospelov, J. Pradler, and A. Ritz, *Phys. Lett. B* **747**, 331 (2015).

[6] B. A. Dobrescu, *Phys. Rev. Lett.* **94**, 151802 (2005).

[7] C. Patrignani *et al.*, *Chin. Phys. C* **40**, 100001 (2016).

[8] B. A. Dobrescu and I. Mocioiu, *J. High Energy Phys.* **11** (2006) 005.

[9] M. Safronova, D. Budker, D. DeMille, D. F. J. Kimball, A. Derevianko, and C. W. Clark, *Rev. Mod. Phys.* **90**, 025008 (2018).

[10] L. Covi, H. Kim, J. Kim, and L. Roszkowski, *J. High Energy Phys.* **05** (2001) 033.

[11] J. Jaeckel and A. Ringwald, *Annu. Rev. Nucl. Part. Sci.* **60**, 405 (2010).

[12] C. T. Hill and G. G. Ross, *Nucl. Phys.* **B311**, 253 (1988).

[13] R. C. Ritter, C. E. Goldblum, W. T. Ni, G. T. Gillies, and C. C. Speake, *Phys. Rev. D* **42**, 977 (1990).

[14] B. R. Heckel, C. E. Cramer, T. S. Cook, S. Schlamminger, E. G. Adelberger, and U. Schmidt, *Phys. Rev. Lett.* **97**, 021603 (2006).

[15] W. A. Terrano, E. G. Adelberger, J. G. Lee, and B. R. Heckel, *Phys. Rev. Lett.* **115**, 201801 (2015).

[16] G. D. Hammond, C. C. Speake, C. Trenkel, and A. P. Patón, *Phys. Rev. Lett.* **98**, 081101 (2007).

[17] J. Long, H. Chan, A. Churnside, E. Gulbis, M. Varney, and J. Price, *Nature (London)* **421**, 922 (2003).

- [18] J. C. Long and V. A. Kostelecký, *Phys. Rev. D* **91**, 092003 (2015).
- [19] G. Vasilakis, J. M. Brown, T. W. Kornack, and M. V. Romalis, *Phys. Rev. Lett.* **103**, 261801 (2009).
- [20] B. R. Heckel, W. A. Terrano, and E. G. Adelberger, *Phys. Rev. Lett.* **111**, 151802 (2013).
- [21] D. J. Wineland, J. J. Bollinger, D. J. Heinzen, W. M. Itano, and M. G. Raizen, *Phys. Rev. Lett.* **67**, 1735 (1991).
- [22] A. K. Petukhov, G. Pignol, D. Jullien, and K. H. Andersen, *Phys. Rev. Lett.* **105**, 170401 (2010).
- [23] H. Yan, G. A. Sun, S. M. Peng, Y. Zhang, C. Fu, H. Guo, and B. Q. Liu, *Phys. Rev. Lett.* **115**, 182001 (2015).
- [24] P.-H. Chu, A. Dennis, C. Fu, H. Gao, R. Khatiwada, G. Laskaris, K. Li, E. Smith, W. M. Snow, H. Yan *et al.*, *Phys. Rev. D* **87**, 011105 (2013).
- [25] K. Tullney, F. Allmendinger, M. Burghoff, W. Heil, S. Karpuk, W. Kilian, S. Knappe-Grüneberg, W. Müller, U. Schmidt, A. Schnabel *et al.*, *Phys. Rev. Lett.* **111**, 100801 (2013).
- [26] A. P. Serebrov, O. Zimmer, P. Geltenbort, A. Fomin, S. Ivanov, E. Kolomensky, I. Krasnoshekova, M. Lasakov, V. M. Lobashev, A. Pirozhkov *et al.*, *JETP Lett.* **91**, 6 (2010).
- [27] F. Ficek, D. F. J. Kimball, M. G. Kozlov, N. Leefer, S. Pustelny, and D. Budker, *Phys. Rev. A* **95**, 032505 (2017).
- [28] C. B. Fu, T. R. Gentile, and W. M. Snow, [arXiv:1007.5008](https://arxiv.org/abs/1007.5008).
- [29] L. R. Hunter and D. G. Ang, *Phys. Rev. Lett.* **112**, 091803 (2014).
- [30] T. M. Leslie, E. Weisman, R. Khatiwada, and J. C. Long, *Phys. Rev. D* **89**, 114022 (2014).
- [31] W. Ji, C. B. Fu, and H. Gao, *Phys. Rev. D* **95**, 075014 (2017).
- [32] T. W. Kornack, R. K. Ghosh, and M. V. Romalis, *Phys. Rev. Lett.* **95**, 230801 (2005).
- [33] Y. Chen, W. Quan, S. Zou, Y. Lu, L. Duan, Y. Li, H. Zhang, M. Ding, and J. Fang, *Sci. Rep.* **6**, 36547 (2016).
- [34] J. Fang, Y. Chen, Y. Lu, W. Quan, and S. Zou, *J. Phys. B* **49**, 135002 (2016).
- [35] J. Fang, Y. Chen, S. Zou, X. Liu, Z. Hu, W. Quan, H. Yuan, and M. Ding, *J. Phys. B* **49**, 065006 (2016).
- [36] M. Smiciklas, J. M. Brown, L. W. Cheuk, S. J. Smullin, and M. V. Romalis, *Phys. Rev. Lett.* **107**, 171604 (2011).
- [37] Y. Chen, [arXiv:1706.08760](https://arxiv.org/abs/1706.08760).
- [38] T. W. Kornack, S. J. Smullin, S.-K. Lee, and M. V. Romalis, *Appl. Phys. Lett.* **90**, 223501 (2007).
- [39] A. S. Krasichkov, E. B. Grigoriev, M. I. Bogachev, and E. M. Nifontov, *Phys. Rev. E* **92**, 042927 (2015).